Am J Physiol Heart Circ Physiol 318: H1162–H1175, 2020.
First published March 27, 2020; doi:10.1152/ajpheart.00094.2020.

RESEARCH ARTICLE | *Integrative Cardiovascular Physiology and Pathophysiology*

Loss of dynamic regulation of G protein-coupled receptor kinase 2 by nitric oxide leads to cardiovascular dysfunction with aging

Melissa Lieu,[1]* Christopher J. Traynham,[1]* Claudio de Lucia,[1] Jessica Pfleger,[1] Michela Piedepalumbo,[1,2] Rajika Roy,[1] Jennifer Petovic,[1] Gavin Landesberg,[3] Steven J. Forrester,[3] Matthew Hoffman,[1] Laurel A. Grisanti,[1,4] Ancai Yuan,[1] Erhe Gao,[1] Konstantinos Drosatos,[1] Satoru Eguchi,[3] Rosario Scalia,[3] Douglas G. Tilley,[1] and Walter J. Koch[1]

[1]*Center for Translational Medicine, Department of Pharmacology, Lewis Katz School of Medicine, Temple University, Philadelphia, Pennsylvania;* [2]*Department of Medical, Surgical, Neurological, Metabolic, and Aging Sciences, University of Campania "Luigi Vanvitelli," Naples, Italy;* [3]*Cardiovascular Research Center, Lewis Katz School of Medicine, Temple University, Philadelphia, Pennsylvania; and* [4]*Department of Biomedical Sciences, College of Veterinary Medicine, University of Missouri, Columbia, Missouri*

Submitted 7 February 2020; accepted in final form 21 March 2020

Lieu M, Traynham CJ, de Lucia C, Pfleger J, Piedepalumbo M, Roy R, Petovic J, Landesberg G, Forrester SJ, Hoffman M, Grisanti LA, Yuan A, Gao E, Drosatos K, Eguchi S, Scalia R, Tilley DG, Koch WJ. Loss of dynamic regulation of G protein-coupled receptor kinase 2 by nitric oxide leads to cardiovascular dysfunction with aging. *Am J Physiol Heart Circ Physiol* 318: H1162–H1175, 2020. First published March 27, 2020; doi:10.1152/ajpheart.00094.2020.—Nitric oxide (NO) and *S*-nitrosothiol (SNO) are considered cardio- and vasoprotective substances. We now understand that one mechanism in which NO/SNOs provide cardiovascular protection is through their direct inhibition of cardiac G protein-coupled receptor (GPCR) kinase 2 (GRK2) activity via *S*-nitrosylation of GRK2 at cysteine 340 (C340). This maintains GPCR homeostasis, including β-adrenergic receptors, through curbing receptor GRK2-mediated desensitization. Previously, we have developed a knockin mouse (GRK2-C340S) where endogenous GRK2 is resistant to dynamic *S*-nitrosylation, which led to increased GRK2 desensitizing activity. This unchecked regulation of cardiac GRK2 activity resulted in significantly more myocardial damage after ischemic injury that was resistant to NO-mediated cardioprotection. Although young adult GRK2-C340S mice show no overt phenotype, we now report that as these mice age, they develop significant cardiovascular dysfunction due to the loss of SNO-mediated GRK2 regulation. This pathological phenotype is apparent as early as 12 mo of age and includes reduced cardiac function, increased cardiac perivascular fibrosis, and maladaptive cardiac hypertrophy, which are common maladies found in patients with cardiovascular disease (CVD). There are also vascular reactivity and aortic abnormalities present in these mice. Therefore, our data demonstrate that a chronic and global increase in GRK2 activity is sufficient to cause cardiovascular remodeling and dysfunction, likely due to GRK2's desensitizing effects in several tissues. Because GRK2 levels have been reported to be elevated in elderly CVD patients, GRK2-C340 mice can give insight into the aged-molecular landscape leading to CVD.

NEW & NOTEWORTHY Research on G protein-coupled receptor kinase 2 (GRK2) in the setting of cardiovascular aging is largely unknown despite its strong established functions in cardiovascular physiology and pathophysiology. This study uses a mouse model of chronic GRK2 overactivity to further investigate the consequences of long-term GRK2 on cardiac function and structure. We report for the first time that chronic GRK2 overactivity was able to cause cardiac dysfunction and remodeling independent of surgical intervention, highlighting the importance of GRK activity in aged-related heart disease.

cardiac hypertrophy; heart disease; *S*-nitrosylation

INTRODUCTION

β-Adrenergic receptor (β-AR) signaling is central to cardiac physiology and disease (16). These prototypic G protein-coupled receptors (GPCRs) respond to sympathetic stimuli to increase cardiac chronotropy, inotropy, dromotropy, and lusitropy. GPCR kinases (GRKs) deactivate agonist-associated β-ARs and other GPCRs in the cardiovascular (CV) system (39, 56). GRK2 is the predominate cardiac GRK isoform and the main isoform implicated in β-AR phosphorylation, desensitization, and downregulation (20, 39, 46, 56). Of importance to CV disease (CVD), GRK2 is upregulated in both expression and activity in the human heart and vasculature following cardiac injury/stress conditions such as ischemia or hypertension (11, 28). This is detrimental as it leads to hyper-desensitization and downregulation of receptors in the failing heart on top of functional abnormalities (56). Research over the last two decades has documented the pathological role of enhanced GRK2 in CVD, including hypertension and heart failure (HF) progression (39, 56). Of clinical importance, CVD prevalence increases drastically with advancing age so that by 80+ years of age up to 91.8% of the US population is afflicted, but research has largely ignored the impact of aging in CVD research (3, 35).

GRK2 has been shown to phosphorylate a growing number of non-GPCR substrates. Additionally, it has been shown to interact with and regulate the function of several critical proteins, comprising an expanding GRK2 "interactome" (49). Thus, the cellular regulation of GRK2 is of interest, which includes posttranslational modifications such as phosphorylation and *S*-nitrosylation (56). Whalen et al. (66) reported that

* M. Lieu and C. J. Traynham contributed equally to this work.
Address for reprint requests and other correspondence: W. J. Koch, Temple Univ. Lewis Katz School of Medicine, Center for Translational Medicine, 3500 N. Broad St., MERB 941, Philadelphia, PA 19140 (e-mail: walter.koch@temple.edu).

GRK2 exists in complex with endothelial nitric oxide synthase (eNOS) and is dynamically *S*-nitrosylated at cysteine 340 (C340) via low molecular weight *S*-nitrosothiols (SNOs). The physiological significance of this eNOS-SNO-GRK2 regulation appears to be an endogenous brake on GRK2, as SNO-GRK2 at C340 inhibits its kinase activity to prevent β-AR desensitization during homeostasis (66). Reciprocally, GRK2 was able to indirectly decrease eNOS activity through reduced eNOS phosphorylation (6, 27), thereby revealing a bidirectional relationship between eNOS and GRK2. A knockin (KI) mouse model, in which C340 of GRK2 was mutated to a serine (GRK2-C340S) to abolish dynamic *S*-nitrosylation, showed heightened global GRK2 activity and reduced eNOS responsiveness (27). Consistent with a pathological role for enhanced GRK2, we found increased cardiomyocyte cell death and cardiac injury following acute ischemia-reperfusion (I/R) injury in the GRK2-C340S KI mice compared with wild-type (WT) control mice, and these mice were also resistant to the cardioprotective properties of nitric oxide (NO) donors (27). However, at baseline young adult (8–15 wk) GRK2-C340S mice otherwise had no obvious basal CV phenotype compared with WT control mice. With previous studies debating the requirement of GRK2 in developing CVD, we hypothesized that GRK2-C340S mice that have chronic unchecked GRK2 activity globally may develop CV remodeling and dysfunction at baseline. Indeed, by 12 mo of age, GRK2-C340S mice develop significant vascular and myocardial pathologies compared with age-matched WT controls. Thus, for the first time, we show that heightened global GRK2 activity due to loss of SNO-mediated endogenous inhibition can independently cause CVD over time.

Given that the population of individuals aged 65 yr and older is estimated to outnumber children by 2030, it is of increasing importance to understand the dynamics between age and CVD. Included is the potential risk of elevated CV GRK2 levels and activity that has been linked with aging (60, 62).

MATERIALS AND METHODS

Experimental animals. All animal procedures were carried out according to the National Institutes of Health's *Guide for the Care and Use of Laboratory Animals* and approved by the Animal Care and Use Committee of Temple University. GRK2-C340S mice expressing endogenous levels of GRK2 with a KI mutation Cys340→Ser were generated as previously described (27). The GRK2-C340S line was maintained on a C57BL6/J background in which WT controls are mice that do not contain the KI mutation from the GRK2-C340S line. The overall age range of old WT and GRK2-C340S mice used in this study were 52–82 wk. Old WT and GRK2-C340S mouse groups within each individual experiment were age matched to highlight phenotypic changes based on genotype. Young mice used were between 8 and 15 wk of age. Both males and females were used for experiments and sex matched.

Echocardiography. All echocardiography was performed using the Vevo 2100 imaging system from VisualSonics as previously described (17, 58). Hair from the mouse chest was removed with Nair >24 h before echocardiography. Mice were anesthetized with 3% isoflurane and maintained at 1–3% during procedures. Traditional echocardiography (TE) used the MS400 (30-MHz centerline frequency) probe to obtain B- and M-mode images from the parasternal long axis and short axis to evaluate left ventricular (LV) internal diameters, fractional shortening (FS), end-diastolic volume (V;d), end-systolic volume (V;s), and heart rate.

Left ventricular deformation was evaluated using echocardiographic speckle tracking-based strain imaging (STE) images from parasternal long-axis B-mode loops consisting of 300 frames at ≥200 frames/s. Images were analyzed using the Vevo Strain Software Vevo LABORATORY 1.7.1. Strain, which is a measure of the change in length, was calculated from the radial axis and longitudinal axis. Strain rate, which is a measure of the change in length over time, was calculated from both axes as well. Strain or strain rate may be presented regionally (basal, mid-, and apical anterior; basal, mid-, and apical posterior) or globally across the whole left ventricle. Reverse longitudinal and radial strain rate measured longitudinal and radial strain during early LV filling (diastole), which was obtained using the "reverse peak" algorithm from Vevo Laboratory 1.7.1. strain.

Diastolic function was evaluated from two-dimensional echo in combination with tissue Doppler and pulsed-wave Doppler from apical long-axis views. With pulsed-wave Doppler spectral waveforms, peak early (*E* wave) and late diastolic (*A* wave) transmittal velocities were obtained to calculate *E*/*A* ratio and isovolumic relaxation time. With tissue Doppler spectral waveforms, early diastolic myocardial relaxation velocity was obtained to calculate E'/E ratio.

Serum catecholamines. Serum epinephrine and norepinephrine levels were measured using Adrenaline Research ELISA and Noradrenaline Research ELISA from Labor Diagnostika Nord GmbH & CO KG according to manufacturer's protocol, respectively. Briefly, blood was collected from the right carotid artery of mice under anesthesia and incubated at room temperature for 30 min. Serum was collected after centrifugation. Sample volumes used were 10 μL for norepinephrine ELISA and 40 μL for epinephrine ELISA.

RNA isolation and qPCR. Total RNA was isolated using TRIzol and the Direct-zol RNA Miniprep Kit (Zymo Research) according to manufacturer's instructions. cDNA was generated from isolated RNA using the iScript cDNA Synthesis Kit (Bio-Rad). Semiquantitative PCR on cDNA was done using SYBR Green (Bio-Rad) and a final concentration of 100 nM of gene-specific oligonucleotides for atrial natriuretic factor (*Nppa*, ANF), brain natriuretic peptide (*Nppb*, BNP), *GRK2*, and *Rn18s* (18S) on a CFX96 Real Time System with BioRad CFX Manager 2.1 software (Bio-Rad). Quantification was done through 18S rRNA normalization and compared using the ΔΔCt method.

Terminal hemodynamics. Briefly, a 1.4-Fr micromanometer-tipped catheter (Millar Instruments) was inserted into the right carotid artery and then advanced into the LV. A polyethylene-50 catheter was placed in the left external jugular vein for continuous infusion of isoproterenol, and an isoproterenol dose response curve was performed as we have done previously (58). Systolic blood pressure was recorded in closed-chest mode throughout the experiment with a PowerLab DAQ System (Millar Instruments).

Isometric aortic contraction assay. Isometric aortic contraction assays were performed as described previously (50). Briefly, thoracic aortas from WT or GRK2-C340S mice were cleaned of surrounding tissue, cut into 2.5-mm rings, and then mounted onto a myograph (Radnoti Wire Myograph, Radnoti LLC). Rings were equilibrated for 60 min before max contraction was measured with KCl (100 mM). After washing out the KCl, phenylephrine (PE) dose response was assessed (1×10^{-9} to 3×10^{-3}M). Rings were precontracted with an EC_{50} concentration of PE before endothelium-dependent relaxation was assessed using acetylcholine (Ach; 1×10^{-9} to 3×10^{-3} M). To evaluate basal tone NO release, rings were incubated with N^G-nitro-L-arginine methyl ester (L-NAME) (50 μM) for 45 min.

Radioligand binding. In brief, crude cardiac membrane preparations were prepared as previously described (50). The total density of expressed β-ARs in cardiac lysates was determined by saturation-binding experiments using the nonselective β-AR antagonist (−)3-[^{125}I]iodocyanopindolol ([^{125}I]CYP) as the radioligand. Propranolol (10 μM) was used to determine nonspecific binding. Amounts of total and nonspecific radiolabel bound to cell membranes were calculated from radioactive counts remaining on the glass fiber filters. From the

plotted saturation hyperbola, β-AR density (B_{max}) and affinity value (K_d) of [^{125}I]CYP for each sample were calculated using iterative nonlinear regression analysis.

Histological sectioning and staining. Renal vascular hypertrophy and perivascular fibrosis were evaluated with Sirius Red (EMS) staining in kidney samples obtained from aged WT and GRK2-C340S. Briefly, after deparaffinization and rehydration, sections (4–5 μm thick) were stained in equal parts Weigart's iron hematoxylin A and B (EMS) for 10 min at room temperature. Sections were washed twice in distilled water for 3 min per wash. Sirius Red was added for 1 h at room temperature. Slides were washed twice in 0.01 N HCl for 3 min per wash. Sections were then dehydrated and penetrated using ethanol and xylene, respectively. Thoracic aortas and hearts were stained with Masson's trichrome to distinguish media area from adventitia and fibrosis, respectively, as previously described (58). Briefly, after deparaffinization and rehydration, sections were incubated with Bouin's fluid for 1 h at 56°C. Sections were washed three times in distilled water for 3 min per wash and incubated with working hematoxylin-eosin solution for 7.5 min, followed by washing in distilled water for 30 s. Sections were then incubated with Biebrich Scarlet-Acid Fuchsin solution for 5 min. After being incubated with phosphotungstic-phosphomolyhdic acid solution for 5 min, sections were stained with Aniline Blue stain solution for 5 min. Sections were washed in 1% acetic acid for 30 s and distilled water for 30 s. To analyze cell cross-sectional area, heart sections were stained with wheat germ agglutinin (WGA; ThermoFisher, 10 μg/mL in PBS) for 1 h in a humidified dark chamber, as described previously (58). Sections were dehydrated and penetrated using ethanol and xylene, respectively. Analysis was conducted using ImageJ software.

Histological quantifications. Cardiomyocyte cell cross-sectional area was quantified as previously described from WGA staining (58). To quantify cardiac fibrosis, multiple images from Masson's trichrome-stained hearts were taken across the left ventricle. The blue stained area (fibrosis) was outlined and quantified. To calculate cardiac perivascular fibrosis, the value of the fibrosis area was subtracted from the value of the vessel area divided by the true area of the vessel. To quantify vascular hypertrophy in the kidney, the value of medial area was divided by the true area of the vessel. True area was calculated by vessel outer perimeter squared divided by 4π. To calculate renal perivascular fibrosis, the value of fibrosis area was subtracted from vessel area and divided by the true area of the vessel. A minimum of three representative vascular images was analyzed per sample. Medial hypertrophy of thoracic aorta was quantified by measurements of medial thickness in four randomly selected locations per slide. A minimum of three representative vascular images was analyzed per biological replicate.

Immunohistochemistry of cardiac sections. Subsequent to heat-induced antigen retrieval, heart sections were immunolabeled with primary antibodies for platelet endothelial cell adhesion molecule (PECAM-1)/cluster of differentiation 31 (CD31) (R&D AF3628) and α-smooth muscle actin (αSMA) (Sigma-Aldrich A5228) as described (10). Secondary fluorophore-conjugated antibodies (ThermoFisher A21432, A21202) were then used to analyze the immunofluorescence. Images throughout the heart were obtained with the Nikon Eclipse Ti-E fluorescence microscope, merged using Adobe Photoshop (Adobe), and analyzed with ImageJ. CD31 and aSMA counts were normalized to tissue area.

Statistical analysis. All values in the text and figures are presented as means ± SE. Statistical significance between two groups was determined by Student's unpaired *t* test. Statistical significance between three or more groups with two or more variables was determined by two-way ANOVA with Tukey's multiple comparisons test. Probabilities of 0.05 or less were considered to be statistically significant. Statistical calculations were done in Prism 7 (GraphPad). Effect sizes for statistically significant differences between two groups are reported as Cohen's *d*, calculated by the mean difference divided by their pooled standard deviation.

RESULTS

Aged GRK2-C340S mice exhibit cardiac dysfunction. WT and GRK2-C340S mice were allowed to age to 2–3 mo (8–15 wk) or 12–20 mo (52–82 wk) before implementation into the young or old study groups, respectively. Old GRK2-C340S mice expressed GRK2 protein at endogenous levels seen in old WT mice, corresponding with our previous study confirming young GRK2-C340S mice also express GRK2 at endogenous levels seen in young WT mice while activity is increased (Supplemental Fig. S1; all supplemental material is available at https://doi.org/10.6084/m9.figshare.11823750.v1) (27). A typical laboratory mouse lifespan is 1.3–3 yr, making our young mice equivalent to ~20–30 human years and our old mice equivalent to ~40–64 human years (19, 23, 65a). As GRK2-C340S mice aged, we observed a steady decline in cardiac function as determined by traditional echocardiography (TE) or speckle tracking-based strain echocardiography (STE). By ≥12 mo of age, GRK2-C340S mice have a significant reduction in ejection fraction (EF) detected by STE compared with age-matched WT counterparts ($d = 1.71$) (Fig. 1*A*). GRK2-C340S groups experienced significant declines in EF over time ($d = 1.63$), but this was only trending in WT groups: young WT = 65.3% versus old WT = 57.5% ($d = 1.00$) (Fig. 1*A*). EFs in old GRK2-C340S males ($d = 1.31$) and females ($d = 2.22$) were significantly declined to the same extent (Supplemental Fig. S2, *A* and *B*). EF and FS obtained by TE showed similar patterns between groups and within groups over time: reduced EF ($d = 1.79$) and FS ($d = 1.78$) in old WT versus old GRK2-C340S; decline in EF and FS in old WT ($d = 1.39$; 1.32) or GRK2-C340S ($d = 2.44$; 2.20) mice versus young mice (Supplemental Fig. S2, *C* and *D*). Left ventricular internal dimensions at systole (LVIDs) ($d = 2.03$) and diastole (LVIDd) ($d = 1.63$) were both significantly increased in old GRK2-C340S mice compared with age-matched WT mice, indicative of LV dilation. Internal diameters were increased in old groups compared with young as well ($d_{WT;s} = 1.80$; $d_{WT;d} = 1.980$; $d_{C340S;s} = 3.37$; $d_{C340S;d} = 3.23$) (Fig. 1, *B* and *C*). Volumes at systole ($d = 1.94$) and diastole ($d = 1.56$) were also significantly increased in old GRK2-C340S mice compared with age-matched WT, which further suggests impaired contractility in aged GRK2-C340S mice (Fig. 1, *D* and *E*). Old WT ($d_{V;s} = 1.83$; $d_{V;d} = 1.98$) and GRK2-C340S ($d_{V;s} = 3.62$; $d_{V;d} = 13.08$) mice had increased volumes compared with their respective young groups, as observed in all other parameters. Additional TE parameters can be found in Supplemental Fig. S2, *E–G*. Measurement of global longitudinal strain (GLS) through STE in aged GRK2-C340S mice revealed that they had significantly greater LV deformation during systole compared with aged WT ($d = 1.61$) (Fig. 1*F*). Further analysis of regional longitudinal or radial strain within the LV revealed similar findings that aged GRK2-C340S cardiac contraction was impaired (Supplemental Fig. S3, *A–E*). Overall, over time GRK2-C340S experience significantly worsened systolic function compared with age-matched WT mice. Declines in systolic function with aging have become more appreciated as advances in echocardiography techniques, i.e., STE, improve its sensitivity (17).

As impaired diastolic function has traditionally been most appreciated to accompany aging, we assessed diastolic function through pulsed-wave Doppler and tissue Doppler echocar-

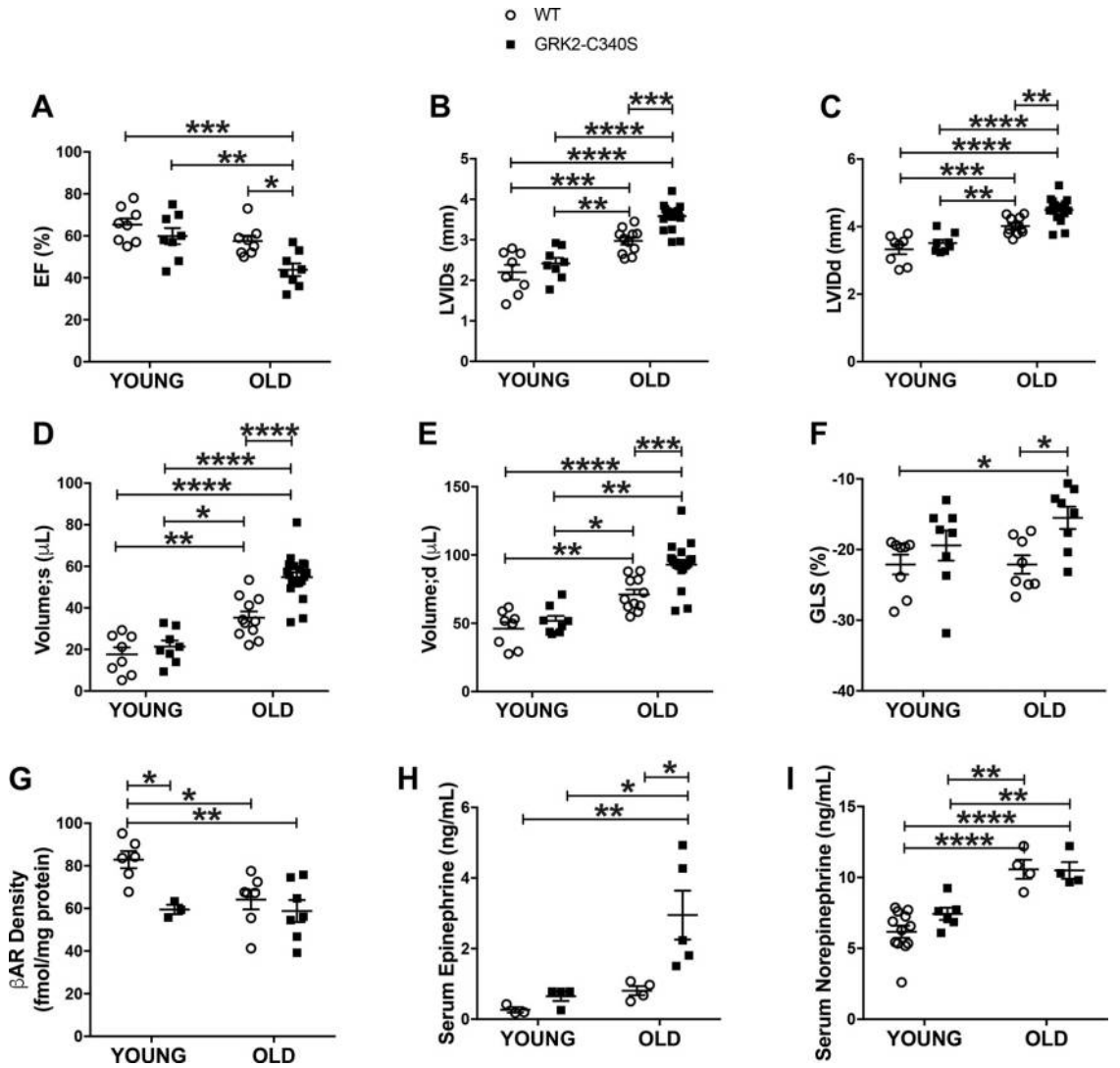

Fig. 1. Aged GRK2-C340S mice have reduced cardiac function. *A*: ejection fraction (EF) from speckle tracking-based strain echocardiography (STE) in young (8–15 wk) and old (52–82 wk) wild-type (WT) or GRK2-C340S mice. Average heart rates during STE are 514, 503, 546, and 509 beats/min ($n = 8$). Left ventricular internal diameters (LVID, mm) of young or aged WT or GRK2-C340S at systole (*B*) and diastole (*C*) obtained by traditional echocardiography (TE). End-diastolic volumes (μL) at systole (*D*) and diastole (*E*) obtained by TE ($n = 8$–20). Average heart rates for TE are 509, 488, 424, and 482 beats/min. *F*: global longitudinal strain (GLS) obtained by STE ($n = 8$). *G*: quantification of β-adrenergic receptor (β-AR) density from radioligand binding assay in cell membranes from young and old WT or GRK2-C340S mice ($n = 3$–7). Serum epinephrine (ng/mL; *H*) ($n = 3$–5) and serum norepinephrine (ng/mL; *I*) ($n = 4$–12) levels measured by ELISA in young and old WT or GRK2-C340S mice. $^*P < 0.05$, $^{**}P < 0.01$, $^{***}P < 0.001$, $^{****}P < 0.0001$ as determined by two-way ANOVA with Tukey's post hoc analysis.

diography. Multiple diastolic indices trended toward impairment in aged GRK2-C340S mice compared with aged WT, including increased isovolumic relaxation time, reduced E/A ratio, reduced E/E′ ratio, and increased LV myocardial performance index compared with age-matched WT controls (Supplemental Fig. S4). Impairments in reverse longitudinal ($d = 1.99$) and radial strain rate ($d = 1.05$) measurements obtained via STE analysis further supported the presence of worsened diastolic function in aged GRK2-C340S mice compared with age-matched WT mice (Supplemental Fig. S3, *F* and *G*). Over time we observed declining cardiac function, congruent with previously published studies in aging (17). Importantly, GRK2-C340S mice with global loss of SNO-mediated GRK2 regulation have significant systolic and diastolic dysfunction that is more pronounced compared with aged WT mice.

GRK2-C340S mice have adrenergic abnormalities. We have previously observed that the loss of SNO regulation on GRK2 in the hearts of GRK2-C340S mice led to overactive GRK2 and enhanced β-AR desensitization with isoproterenol challenge (27). To determine if the cause of decreased cardiac function stemmed from cardiac β-AR abnormalities, β-AR density was measured by radioligand binding of cardiac membranes. A decrease in β-AR density was observed in young GRK2-C340S mice compared with young WT (Fig. 1*G*). However, as previously established, young WT mice do not show cardiac dysfunction at baseline, suggesting that reduced β-ARs alone was not sufficient to produce dysfunction. β-AR density was reduced in both aged groups compared with young WT mice but to the same extent ($d_{WT} = 1.70$; $d_{C340S} = 2.02$) (Fig. 1*G*). Although young GRK2-C340S mice have reduced β-AR expression that is maintained over time, it does not

appear to be the primary contributor to the developing cardiac dysfunction.

Next, we looked at serum catecholamine levels because sympathetic nervous system activation is a hallmark of CVD, including heart failure, and accompanies β-AR desensitization and downregulation (42). Furthermore, catecholamines have been shown to increase over time (13). Of note, we found significantly elevated serum levels of epinephrine in aged GRK2-C340S mice compared with age-matched controls ($d = 1.93$) (Fig. 1*H*). Norepinephrine was significantly elevated in aged groups compared with young groups ($d_{WT} = 3.08$; $d_{C340S} = 2.72$) but with no apparent difference within groups (Fig. 1*I*). The increased serum epinephrine is of physiological significance because we have previously shown GRK2 activity to be critically important in the release of this catecholamine from the adrenal medulla, as increased activity does lead to increased epinephrine levels (41).

Aged GRK2-C340S mice exhibit adverse cardiac and renal remodeling. Changes in LV function are strongly associated with cardiac remodeling (37, 54). Therefore, we examined the cardiac morphology in old GRK2-C340S mice. Old GRK2-C340S mice presented with hypertrophied hearts observed by significantly increased heart weight-to-body weight (HW/BW) ratios ($d = 1.64$) as well as heart weight-to-tibia length (HW/TL) ratios ($d = 1.13$) compared with aged WT (Fig. 2, *A* and *B*). There is also a striking increase in HW/BW and HW/TL in young versus old GRK2-C340S ($d = 1.47$; $d = 2.92$) mice that is significantly more pronounced than WT mice over time

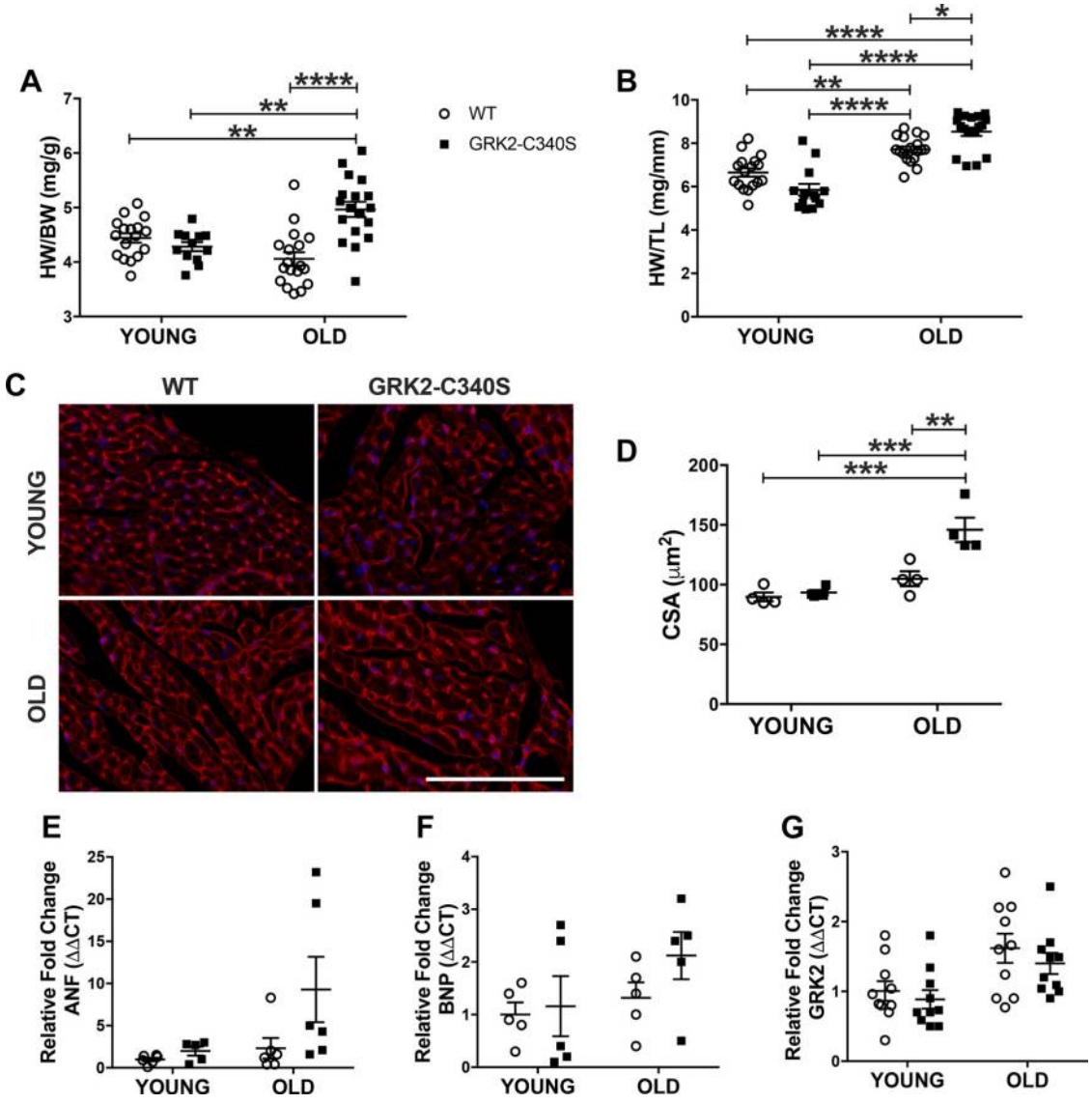

Fig. 2. Aged GRK2-C340S mice exhibit cardiac hypertrophy. Measures of heart weight (HW)-to-body weight (BW) ratios (*A*) and HW-to-tibia length (TL) ratios (*B*) between young and old wild-type (WT) or GRK2-C340S mice ($n = 12$–18). *C*: representative images of wheat germ agglutinin (WGA; red) and 4′,6-diamidino-2-phenylindole (DAPI; blue)-stained young and old WT or GRK2-C340S mouse heart sections. Scale bar, 100 μm. *D*: quantification of cardiomyocyte cross-sectional area (CSA) from WGA staining in young and old WT or GRK2-C340S hearts ($n = 4$). Quantification of qRT-PCR data in young and old WT or GRK2-C340S hearts showed fold change in mRNA expression of atrial natriuretic factor (ANF) (*E*), brain natriuretic peptide (BNP) (*F*) ($n = 5$–6), and GRK2 ($n = 11$) (*G*). *$P < 0.05$, **$P < 0.01$, ***$P < 0.001$,****$P < 0.0001$ as determined by two-way ANOVA with Tukey's post hoc analysis.

($d = 0.86$; $d = 1.51$) (Fig. 2, *A* and *B*). HW/BWs in WT mice do not appear to increase over time, but rather trend to be lower, likely due to large increases in BW with age that masks present physiological heart growth. Hypertrophy was due to increased cardiomyocyte size, as measured from cardiomyocyte cross-sectional area (CSA) through wheat germ agglutinin (WGA) staining. CSA increased in both aged WT ($d = 1.46$) and GRK2-C340S ($d = 3.55$) groups compared with their young counterparts (Fig. 2, *C* and *D*). Aged GRK2-C340S mice displayed more pronounced and significant hypertrophy compared with aged WT ($d = 2.40$) (Fig. 2, *C* and *D*). Trending increased expression of ANF (Fig. 2*E*), BNP (Fig. 2*F*), and GRK2 mRNA (Fig. 2*G*) in GRK2-C340S mice supports this hypertrophy being pathological in nature.

Previous transaortic constriction (TAC) studies in mice with cardiac-specific overexpression of GRK2 (TgGRK2), overexpression confirmed in Supplemental Fig. S5*G*, have shown that TgGRK2 mice hypertrophy to the same extent as their nontransgenic littermate controls (NLCs), despite having increased GRK2 expression and activity (58). To determine whether cardiac GRK2 was specifically responsible for the GRK2-C340S phenotype, we aged TgGRK2 mice to 73 wk. Although old TgGRK2 hearts did hypertrophy over time, it was no different than age-matched NLCs as measured through HW/BW, HW/TL, and CSA (Supplemental Fig. S5, *A–D*). Maladaptive hypertrophic markers, ANF and BNP, between aged TgGRK2 and NLC animals were unchanged (Supplemental Fig. S5, *E* and *F*). Like aged WT controls, aged NLC animals did not show any notable increase in ANF or BNP compared with young counterparts. Additionally, aged TgGRK2 mice also did not experience any declines in EF, measured through TE, compared with age-matched WT mice (Supplemental Fig. S2H). Overall, GRK2-C340S mice develop maladaptive cardiac remodeling over time beyond what is physiologically normal, likely due to noncardiomyocyte unchecked GRK2 activity because TgGRK2 do not show signs of maladaptive remodeling or dysfunction.

As hearts age physiologically, there are changes in the vasculature, including increased fibrosis (4). Examination of the vasculature in aged GRK2-C340S hearts through Masson's Trichrome revealed significantly increased perivascular fibrosis compared with aged WT hearts ($d = 2.03$) (Fig. 3, *A* and *B*). Additionally, perivascular fibrosis increased over time in both WT ($d = 3.47$) and GRK2-C340S ($d = 4.77$) mice but was more pronounced in the latter. Decreases in capillary density with age have been previously reported predominantly in the brain, but they have been reported in the heart and skeletal muscle as well (25, 38, 43, 63). To examine whether there were any changes in vascular density over time due to increased GRK2 activity, immunohistochemistry on heart sections was done with CD31 to mark all vessels, including capillaries, and αSMA to mark larger vessels (arteries, arterioles, veins, and venules). We observed a trend toward decreased CD31 density over time in WT mice and significantly in GRK2-C340S mice ($d = 2.23$) (Fig. 3, *C* and *D*). Similar findings were observed in αSMA density over time (Fig. 3*E*).

Given that the renal system is closely linked to the cardiovascular system so that pathology in one organ increases the risk of pathology in the other and vice versa, we investigated whether the vasculature in the kidneys was also abnormal (1, 12, 40). Histological examination of the kidneys by Sirius Red staining of aged GRK2-C340S mice revealed an increase in vascular medial thickness shown by an increase in vascular medial area to internal arterial area ratio in renal vessels compared with age-matched WT mice ($d = 8.15$) (Fig. 4, *A* and *B*). Moreover, we found that aged GRK2-C340S mice had significantly more renal perivascular fibrosis compared with aged WT mice, parallel to what was observed within the cardiac vasculature ($d = 6.36$) (Fig. 4, *A* and *C*). Thus, aged GRK2-C340S mice exhibit adverse remodeling not only in the myocardium, but also in the kidneys that include significant perivascular fibrosis and vascular hypertrophy. This perivascular fibrosis is evident in multiple organs and highlights the vasculature's vulnerable nature to GRK2 activity. Pathological signaling and remodeling due to upregulated GRK2 activity in the vasculature may be a significant cause of the GRK2-C340S phenotype. Overall, aged GRK2-C340S mice displayed significant multiorgan perivascular fibrosis, renal vascular hypertrophy, and decreased cardiac vessel density over time.

Aged GRK2-C340S mice have increased cardiac pressures. With increased perivascular fibrosis, we next examined aged GRK2-C340S mice hemodynamically to give insights on vascular function. Young mice had no differences in blood pressure (Fig. 5*A*). Consistent with elevated sympathetic nervous system activity, we found that aged GRK-C340S mice had significantly higher systolic pressures at baseline compared with aged WT mice within the left ventricle ($d = 0.94$) (Fig. 5*B*). Aged GRK2-C340S mice continued to display significantly elevated pressures during β-adrenergic challenge with isoproterenol compared with aged WT mice ($d_{0.01ng} = 3.31$; $d_{0.05ng} = 3.49$; $d_{1ng} = 3.71$; $d_{5ng} = 3.10$; $d_{10ng} = 3.32$) despite the young groups being no different (Fig. 5, *C* and *D*).

We also investigated whether peripheral blood pressures were concomitantly elevated through two methods: *1*) telemeter inserted in the left carotid artery for 3 days and *2*) BP2000 Blood Pressure Analyzer, representing a noninvasive tail-cuff method. Although both methods did not reveal any statistically significant differences in the individual parameters of systolic and diastolic pressure, there was a trend toward narrowed pulse pressure ($P = 0.08$) (Supplemental Fig. S6). This phenotype is of interest as reduced pulse pressure has been linked to advanced HF and independently predicts mortality, a reflection from poor cardiac function (69). Increases in pulse pressure windows have also been associated with CVD, but more so with mild HF (69).

Aged GRK2-C340S mice exhibit abnormal aortic morphology. Given that aged GRK2-C340S mice had increased LV pressures and significant multiorgan perivascular fibrosis, we took a closer look at the aortic morphology within these mice. This is especially important because the eNOS machinery is prevalent in vessels, and the unchecked GRK2 activity via the loss of SNO regulation will lead to a loss of eNOS activity as we have previously shown (27). We examined aortic sections with Masson's trichrome staining from young and old WT and GRK2-C340S mice. Aged KI mice had significantly reduced medial thickness compared with aged WT aortas ($d = 3.06$), seemingly through a reduction in vascular smooth muscle cells (VSMC) (Fig. 6, *A* and *B*). Surprisingly, young GRK2-C340S mice presented with the same phenotype of reduced medial thickness ($d = 2.70$). Although aortic abnormalities are observed at early time points, they do not produce any functional consequences until seemingly at later time points.

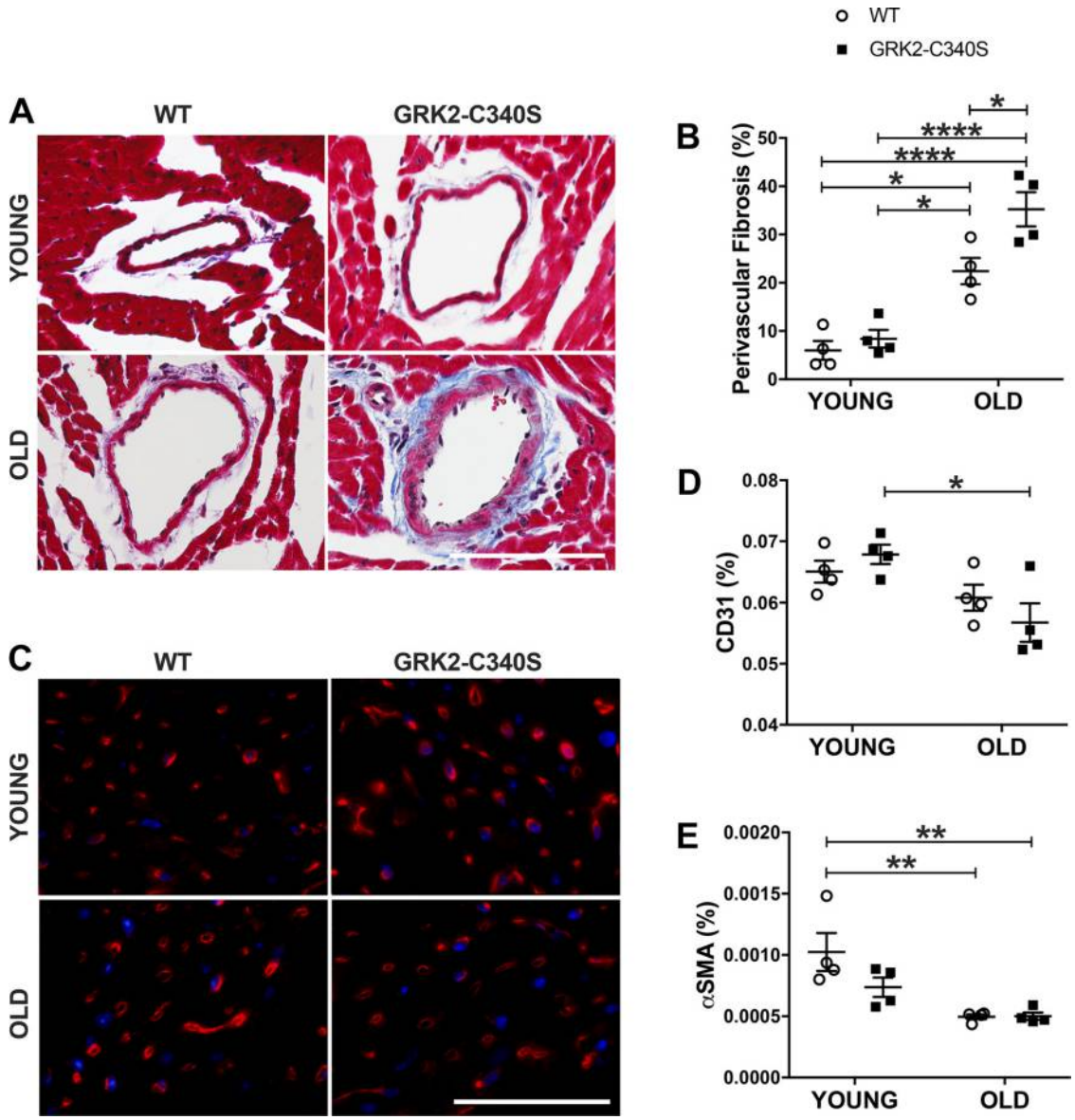

Fig. 3. Aged GRK2-C340S mice exhibit cardiac vascular abnormalities. *A*: representative images of Masson's trichrome-stained aged wild-type (WT) or GRK2-C340S mouse heart sections. Scale bar, 100 μm. *B*: quantification of perivascular fibrotic area in young or aged WT and GRK2-C340S hearts ($n = 4$). *C*: representative images of young and old WT or GRK2-C340S cardiac sections immunolabeled with cluster of differentiation 31 (CD31) (red). Nuclei (blue) were stained with 4′,6-diamidino-2-phenylindole (DAPI). Scale bar, 50 μm. *D*: quantification of CD31 density expressed as a percentage of CD31 positive vessels per tissue area ($n = 4$). *E*: quantification of α-smooth muscle actin (αSMA) density expressed as a percentage of αSMA positive vessels per tissue area ($n = 4$). $^*P < 0.05$, $^{**}P < 0.01$, $^{****}P < 0.0001$ as determined by two-way ANOVA with Tukey's post hoc analysis.

Additionally, they could be a driving force further supporting a potential vasculature origin of GRK2-mediated CV dysfunction. These morphological changes begin at an early age and could result in pressure gradients that could induce the hypertrophic and fibrotic changes we found in the hearts of aged GRK2-C340S mice above. These data suggest that aged GRK2-C340S aortas are overall smaller or narrower than their WT counterparts. Thus, the loss of cardiac function observed in aged GRK2-C340S likely was a result of global, likely cardiac independent, differences in GRK2 activity through loss of *S*-nitrosylation that originated in the vasculature, which resulted in reduced vascular media and smaller aortic dimensions.

Aged GRK2-C340S mice have impaired aortic contractile function. Given that aged GRK2-C340s mice have reduced VSMCs within their media and significant perivascular fibrosis, we examined whether this caused any changes in aortic contractile properties. Aortic rings were isolated from young or old WT, and GRK2-C340S mice were then placed in tissue baths. Upon 100 mM KCl incubation, aortic rings from young WT and GRK2-C340S mice responded with the same force of contraction (Fig. 7*A*). However, aged GRK2-C340S aortas displayed significantly reduced contraction compared with aged WT ($d = 1.51$) (Fig. 7*B*). Similar impaired contraction responses were seen with the α-AR agonist phenylephrine (PE), as contraction was similar in young WT and GRK2-

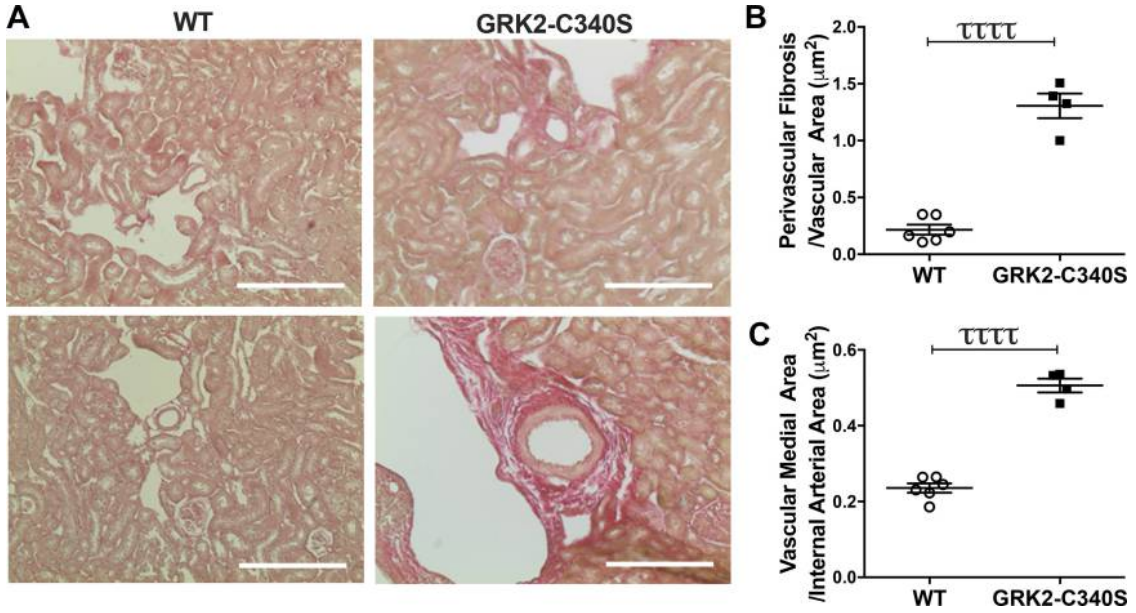

Fig. 4. Aged GRK2-C340S mice develop renal vascular hypertrophy and fibrosis. *A*: representative higher magnification (×100) images of Sirius Red stained aged kidneys from wild-type (WT) and GRK2-C340S mice demonstrating perivascular fibrosis. Scale bar, 100 μm. *B*: quantification of vascular medial area-to-internal arterial area ratio as a measure showing increased medial hypertrophy in aged GRK2-C340S mice compared with WT. *C*: quantification of perivascular fibrosis-to-vascular area ratio from Sirius Red staining in aged WT and GRK2-C340S mice ($n = 4–6$). $\tau\tau\tau\tau P < 0.0001$ as determined by Student's *t* test.

C340S aortas but significantly reduced in aged GRK2-C340S mouse aortas ($d_{10}{}^{-7}{}_{M} = 0.86$; $d_{10}{}^{-6.5}{}_{M} = 0.92$; $d_{10}{}^{-6}{}_{M} = 0.97$; $d_{10}{}^{-5.5}{}_{M} = 1.08$) (Fig. 7, *C* and *D*). Relaxation responses in precontracted rings to acetylcholine were identical in WT and GRK2-C340S mice regardless of age (Fig. 7, *E* and *F*). As strong evidence for the loss of SNO-mediated GRK2 regulation responsible for these vascular contractile changes, we challenged rings with the eNOS inhibitor L-NAME to induce loss of NO. Aortic rings from young WT and GRK2-C340S mice had similar contractile responses due to the loss of the vasorelaxant NO (Fig. 7*G*). However, aortas from aged GRK2-C340S mice had significantly impaired responses to L-NAME compared with age-matched WT mice ($d = 0.80$), demonstrating the importance of SNO-mediated GRK2 inhibition in the vascular contractile response (Fig. 7*H*).

DISCUSSION

GRK2 has been studied for decades and been established as a critical pathological kinase in CVD. We see that in animal

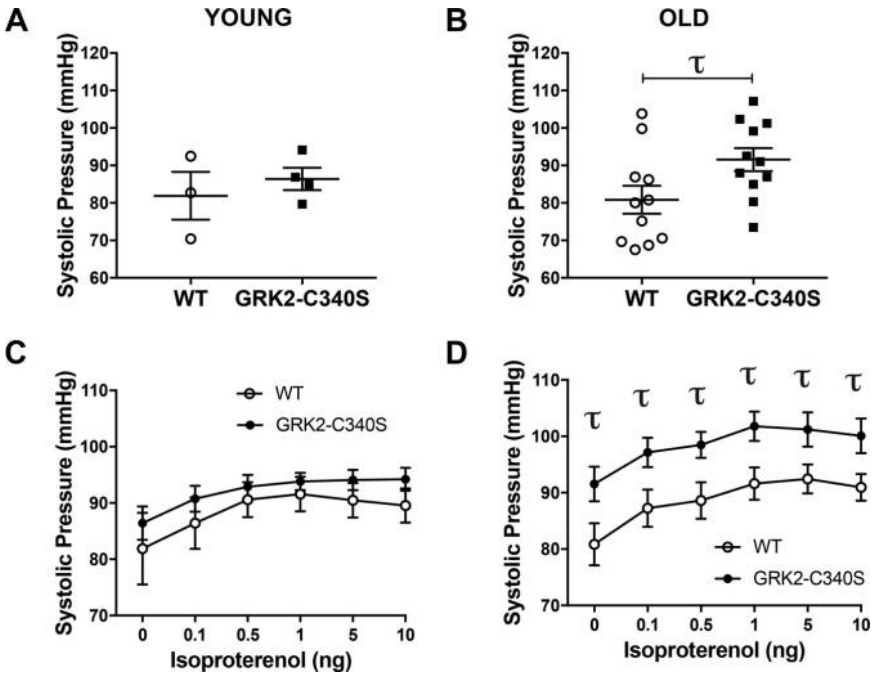

Fig. 5. Aged GRK2-C340S mice exhibit increased blood pressures. Invasive hemodynamic analysis of wild-type (WT) or GRK2-C340S mice within the left ventricle: systolic pressure (mmHg) at baseline in young (*A*) and old (*B*) mice; systolic blood pressure (mmHg) in young (*C*) and old (*D*) mice in response to isoproterenol (0–10 ng) ($n = 11$) $\tau P < 0.05$, as determined by Student's unpaired *t* test between WT compared with GRK2-C340S.

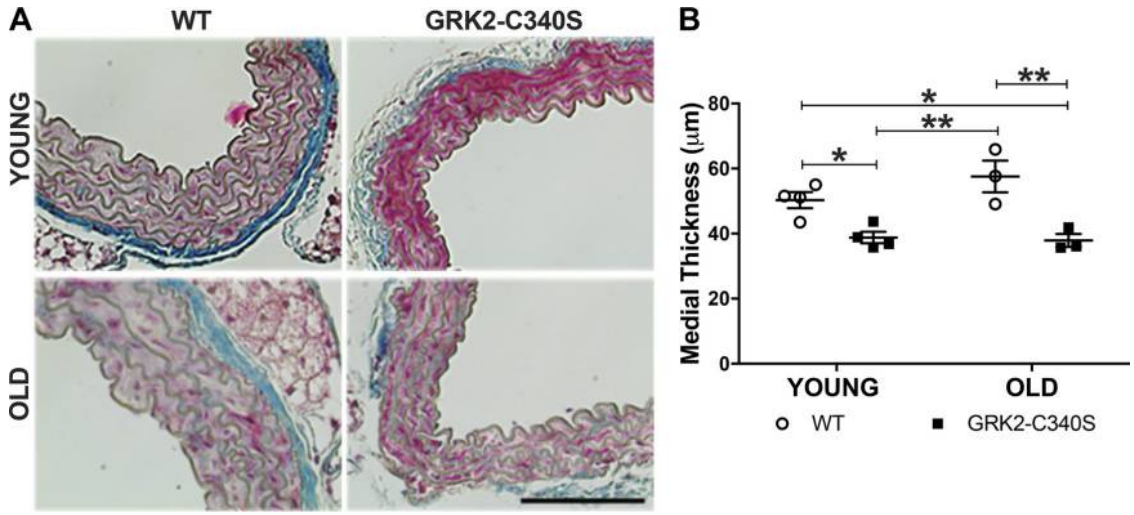

Fig. 6. Aortic size is reduced in aged GRK2-C340S mice *A*: representative images of Masson trichome-stained aged aortas from wild-type (WT) and GRK2-C340S mice demonstrating reduced medial thickness in GRK2-C340S mice. Scale bar, 100 μm. *B*: quantification of medial thickness from Masson trichrome staining in young and old WT and GRK2-C340S mouse aortas ($n = 3–4$). *$P < 0.05$, **$P < 0.01$ as determined by two-way ANOVA with Tukey's post hoc analysis.

models subject to cardiac injury [MI, I/R, and transaortic constriction (TAC)] GRK2 expression and/or activity increase and contribute to cardiac dysfunction and myopathy (39). How GRK2 initiates maladaptive signaling pathways in the heart and related tissues or contributes to the changing molecular landscape over time remain pertinent research questions as we continue to understand GRK2's functions. In this study, we allowed GRK2-C340S mice that lack dynamic SNO-GRK2 regulation, an endogenous mechanism for attenuating GRK2 activity, to age at least 12 mo before enrollment. This unique mechanism of GRK2 activation in GRK2-C340S mice plus aging allowed us to investigate the consequences of global GRK2 overactivity that may not be observed using other GRK2 mouse models. The use of mice ranging from 12–20 mo may not be old enough to significantly recapitulate all hallmarks of aging compared with 24- to 36-mo-old mice used in traditional aging studies (14, 71), but we are primarily concerned with the effects of long-term GRK2 overactivity on the cardiovascular system. For example, we see significant increases in LV hypertrophy and activation of neurohormonal signaling but only trends in declining diastolic function. Overall, we report that chronic GRK2 overactivity is sufficient in causing significantly worsened cardiovascular parameters compared with WT mice, which can provide insights into how GRK2 participates in CVD development, including during intrinsic aging. A summary of our findings in the GRK2-C340S mouse is reviewed in Fig. 8.

It is debated whether GRK2 has a direct mechanistic role in inducing cardiomyocyte hypertrophy in mice (39). Multiple in vitro studies have shown overexpressing GRK2 is sufficient to upregulate hypertrophic gene markers (i.e., ANF, BNP, β-myosin heavy chain) or hypertrophic genes (i.e., nuclear factor of activated T cells and nuclear factor κ-light-chain-enhancer of activated B cells) and increase cell size in cardiac cell lines (57, 65). However, animal models with GRK2 manipulation largely have not translated these findings. For example, we have previously shown cardiac-specific GRK2 overexpressing transgenic (TgGRK2) mice do not experience any changes in cardiac mass after TAC surgery compared with NLCs (58). Of note, these studies enrolled TgGRK2 animals at 8–10 wk of age, which would not take into account changes in the molecular landscape over time. Studies involving GRK2 inhibition in cardiac hypertrophy animal models present with conflicting results, making it difficult to conclude whether cardiac GRK2 can primarily cause hypertrophy (39). Furthermore, transgenic mice with cardiac-specific expression of the βARKct, a GRK2 peptide inhibitor, underwent TAC and hypertrophied to the same degree as NLC mice (8, 58). Kamal et al. (31) reported that inhibition of GRK2 through gallein was able to ameliorate hypertrophy in TAC-operated mice compared with sham. Gallein being a small molecule delivered systemically would make it difficult to differentiate whether its effect was from inhibition of cardiac myocyte GRK2 or from other cell types. Gallein's highly homologous structural analog, M119, was also able to inhibit phospholipase C activation, which could be another mechanism to explain hypertrophic protection from gallein (5). In the present study, we demonstrated that 73-wk-old cardiac TgGRK2 animals still do not experience hypertrophy any differently than NLCs over time. Unchanged cardiac hypertrophy in aged TgGRK2 was represented by unchanged HW/TL ratios, hypertrophic gene expression, and cardiomyocyte cross-sectional area compared with NLC. However, the GRK2-C340S KI mouse with global overactivation of GRK2 did present with cardiac hypertrophy over time. This supports the idea that cardiomyocyte pools of GRK2 may not be directly responsible or sufficient to elicit cardiac hypertrophy in vivo, which agrees with our previous studies demonstrating young TgGRK2 and βARKct mice hypertrophy to the same extent as NLC mice after TAC (29, 58). Currently, there have been no studies investigating the effect of TAC on aged TgGRK2 or TgβARKct mice, but this is something worth future study. However, TAC has been performed on aged WT rodents to investigate the effects of aging on cardiac stress responses. Old age during TAC has been reported to augment pressure overload adaptations in a number of ways, but hypertrophic responses across studies were minimal, if present at all, likely

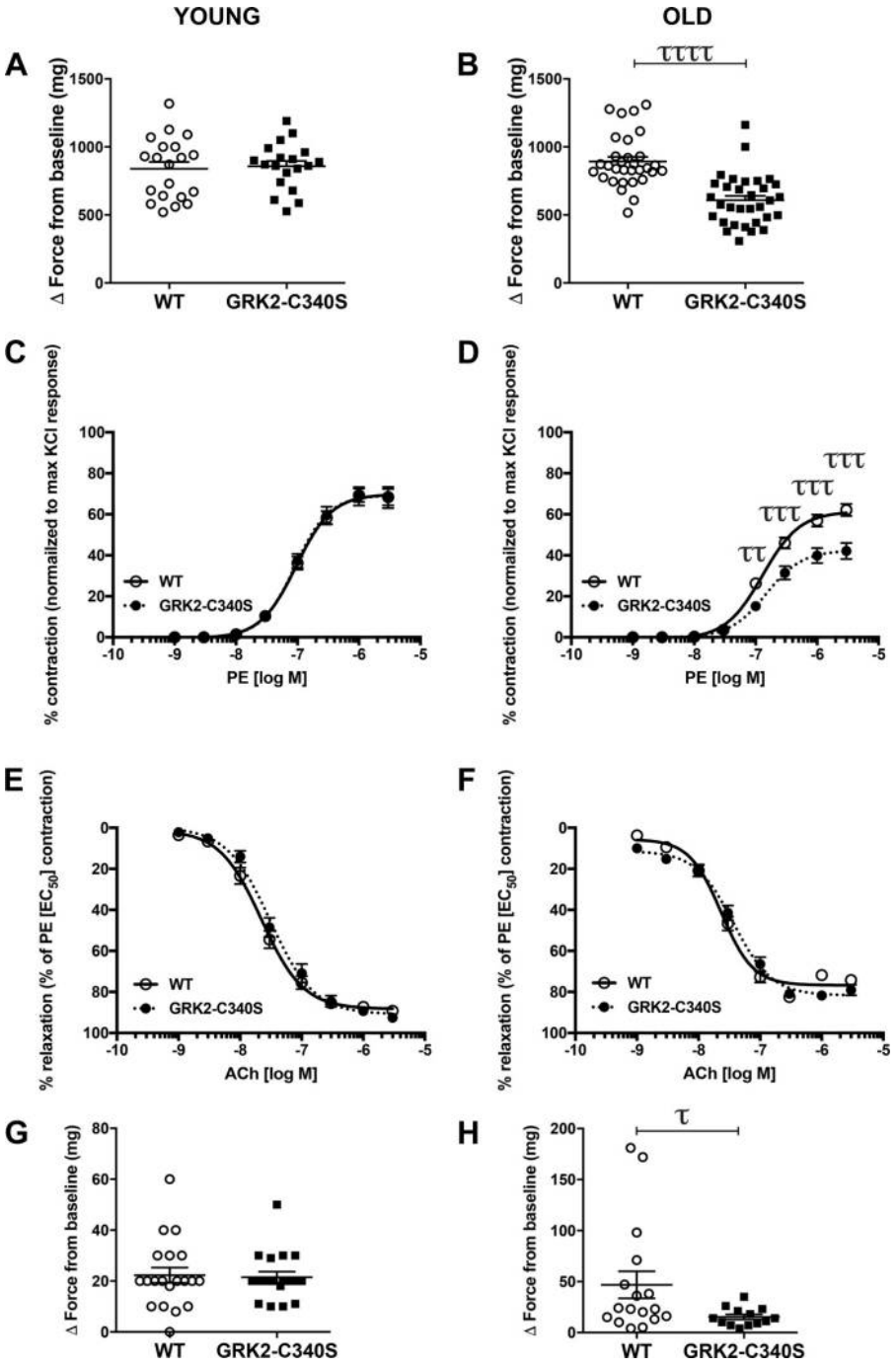

Fig. 7. Aged GRK2-C340S mice exhibit aortic contraction dysfunction. There were 2–4 aortic sections analyzed from each mouse to obtain isometric contractility from baseline of aortic rings with 100 mM KCl incubation from young ($n = 5$) (*A*) and aged ($n = 8$) (*B*) wild-type (WT) (white circles) or C340S mice (black squares). Contractile dose response curves to phenylephrine (PE) in young ($n = 5$) (*C*) and old ($n = 8$) (*D*) WT or C340S aortic rings. Relaxation dose-response curves to acetylcholine in young ($n = 5$) (*E*) and old ($n = 8$) (*F*) WT or C340S aortic rings. Contractility from baseline of aortic rings with 50 μM N^G-nitro-L-arginine methyl ester (L-NAME) incubation from young ($n = 5$) (*G*) and aged ($n = 4$–5) (*H*) WT (white circles) or C340S mice (black squares). $\tau P < 0.05$, $\tau\tau P < 0.01$, $\tau\tau\tau P < 0.001$, $\tau\tau\tau\tau P < 0.0001$ as determined by Student's unpaired *t* test between WT and GRK2-C340S.

due to reduced overall protein production (24, 30, 64). It is clear that aging changes the molecular landscape so that cardiac stress responses will be different compared with young subjects. It is difficult to hypothesize how aged TgGRK2 or βARKct will respond to TAC given these distinctions, but GRK2 activity is likely to have no effect on hypertrophy while still worsening cardiac function. Despite increased GRK2 activity being detrimental to cardiac function during stress (i.e., isoproterenol challenge, TAC surgery), TgGRK2 mice do not experience declines in EF over time like the GRK2-C340S mice, likely due to the eNOS pathway being intact in TgGRK2 animals.

Noncardiomyocyte pools of GRK2 may be more likely the cause for our hypertrophic phenotype observed. Our data suggest GRK2 activity in adrenal glands and vasculature is the culprit for initiating maladaptive hypertrophic signaling in the heart. Indeed, other animal models with elevated serum catecholamine levels from non-GRK2 manipulations or chronic β-AR stimulation develop cardiac hypertrophy over time (29, 44). Increased serum epinephrine trending in young knockin mice and significantly elevated in old KI mice is consistent with increased GRK2 activity in the adrenal medulla where desensitization of α_2-ARs have been observed (41). Increased GRK2 activity seems to play a role in perivascular collagen

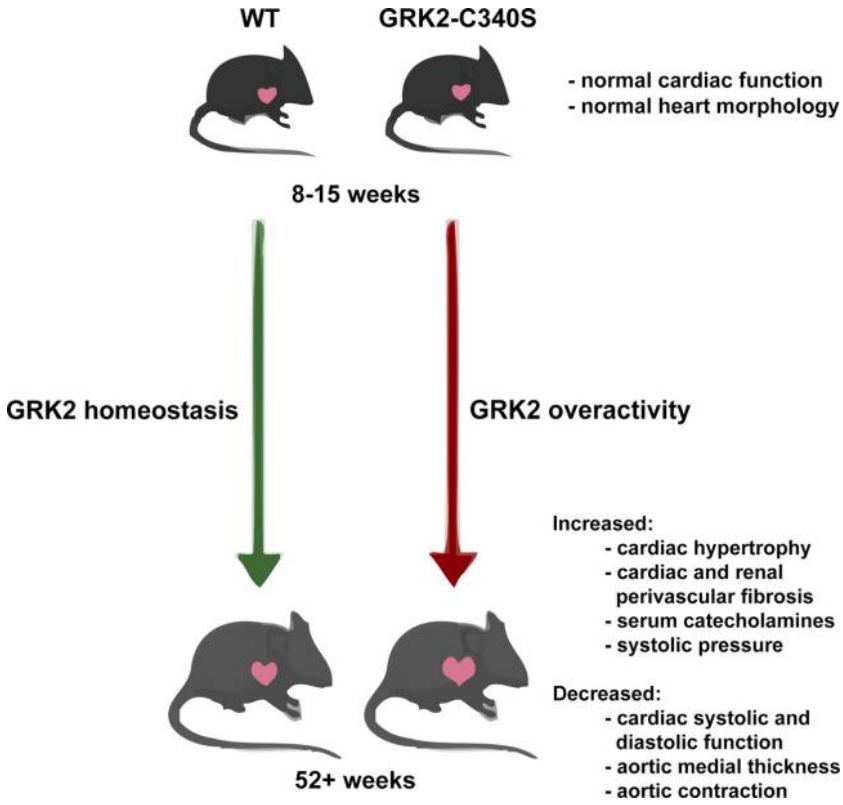

Fig. 8. Summary of aged GRK2-C340S phenotype. Illustration summarizing the age-dependent cardiovascular changes as a result of hyperactive GRK2 from loss of dynamic *S*-nitrosylation negative regulation in the GRK2-C340S mouse. At young ages, wild-type (WT) and GRK2-C340S cardiovascular function and structure are indistinguishable, save for reduced aortic medial thickness in GRK2-C340S mice that is maintained. Over time, increased GRK2 activity causes cardiovascular pathology beyond what is observed in normal physiological aging in WT mice. Aged GRK2-C340S mice present with increased cardiac hypertrophy, cardiac and renal perivascular fibrosis, serum catecholamines, and systolic pressure. Cardiac and aortic function decline in aged GRK2-C340S mice compared with aged WT. GRK2 overactivity in the vasculature and adrenals is likely to play an important role in the overall cardiovascular phenotype observed. Modified from images from Servier Medical Art (http://smart.servier.com/), licensed under a Creative Common Attribution 3.0 Generic License.

deposition and hypertension. In addition to fibroblasts, multiple cell types have been implicated in perivascular fibrosis development, including smooth muscle cells, endothelial cells, pericytes, and immune cells (70). The ability of the heart to deliver oxygen-rich and nutrient-rich blood is subject to cardiac vessel compliance, which perivascular fibrosis greatly impairs (15). Of note, fibrosis during hypertension begins in the perivascular space (70). Vascular stiffness itself increases the risk of stroke and myocardial infarction (45, 55). Both aging and hypertension are known risk factors of vascular stiffness, and indeed our aged GRK2-C340S mice presented with higher systolic blood pressures in the left ventricle compared with aged-matched controls at baseline and during β-AR stimulation. Roles for GRK2 in endothelial and vascular smooth muscle cell physiology have been previously identified. Loss of GRK2 in endothelial cells impaired vasorelaxation, increased macrophage infiltration, and increased collagen degradation from increased matrix metallopeptidase 2 and 9 expression (9). Interestingly, antagonizing GRK2 through systemic administration of M119 in an ISO model of HF reduced perivascular fibrosis compared with ISO treatment alone (7). Vascular smooth muscle (VSM) specific overexpression of GRK2 in mice (TgSM22α-GRK2), 2- to 4-mo-old, presented with significant increases in peripheral blood pressures compared with this study (21). TgSM22α-GRK2 have ~80% increase in GRK2 expression compared with NLC and aortic primary smooth muscle cells derived from these mice have ~300% increase, both leading to increased GRK2 activity as well (21). Although GRK2-C340S mice do have increased global GRK2 activity including the VSM, we may not see such dramatic increases in peripheral blood pressure due to lack of transgenic overexpression and the existence of other GRK2 regulatory pathways beyond *S*-nitrosylation. It is likely that the increase in GRK2 activity observed in GRK2-C340S mice is far less than in TgSM22α-GRK2. Eckhart et al. (21) did not report on whether there were any changes in perivascular fibrosis or vascular density in TgSM22α-GRK2 mice, but VSM-specific GRK2 overexpression was sufficient in inducing myocardial hypertrophy measured by increased HW/BW ratio. Mice with VSM-specific knockout of GRK2 did not observe any changes in heart size at baseline compared with controls and hypertrophied to the same extend as controls in a renal stenosis model of hypertension (11). The impact of GRK2 on vessel density remains a gap in knowledge, but it has been reported that hypertrophic cardiomyopathy patients have reduced arteriolar density (61). Overall, it is evident that GRK2 plays an important role in vascular and adrenal physiology and has a mechanistic role in producing the cardiovascular effects observed in the aged GRK2-C340S mice.

Over the course of a lifetime, there is progressively increasing disorder molecularly, structurally, and functionally due to age that is ironically exacerbated by the body's compensatory mechanisms to preserve function (34, 35). Therefore, the impact of age-related changes on the CV landscape cannot be underestimated when it comes to studying CVD therapies and mechanisms, especially when prevalence and risk of CVD continue to increase after adult onset (≥20 yr) (3). GRK2's role in aging is another area of research that remains obscure within the CV system, but one that demands more research considering CVD is marked with GRK2 activity and patients are predominantly elderly. The few existent studies suggest GRK2 is increased in expression and activity in the aging rat aorta and carotid artery but not in lymphocytes (36, 60). This may not be surprising considering normal physiological aging

is characterized by β-AR system alterations, such as including increased circulating catecholamines, reduced β-AR density, increased β-AR desensitization, increased Gi_{α} protein and signaling, and decreased contractility (13, 22). GRK2 has been established to directly cause all of the above during CVD via phosphorylating β-ARs (16). Increased GRK2 expression has also been reported in aged rat livers and aged human brains (48, 62). As GRK2 levels increase over time and are elevated in CVD, the GRK2-C340S mouse presents with a chronic disease phenotype that considers CVD and age, which can be a valuable tool. GRK2's role in aging demands more research in the future to comprehensively understand its contribution. GRK2 remains an attractive therapeutic target, and multiple efforts have been made to inhibit its activity, including pharmacologically (31, 59), virally (51, 53, 67), and genetically (32, 52). Anti-GRK2 therapy may be beneficial not only during CVD, but perhaps as a cardiac preventative measure as well.

Limitations. Besides the limited current research available for GRK2 in aging, this present study has other limitations. The phenotype of reduced medial thickness, seemingly from reduced smooth muscle content, in our GRK2-C340S mice was unexpected and incongruent with phenotypes in aging models and humans. Aging does cause vascular structural remodeling, but it comprises collagen accumulation, decreased elastin, and VSMC proliferation within the media (68). The mechanism resulting in this unique phenotype would require further investigation. The seemingly smaller aortas may be the cause of reduced pulse pressure. Reduced pulse pressure can be observed in settings of aortic narrowing, like aortic stenosis or aortic coarctation, although there can be high heterogeneity between patients and dependence on severity (2, 26). Our aortic phenotype remains histologically different compared with aortic stenosis or coarctation, but we do observe parallels within our present data, i.e., high pressures above the aorta and lower pressures below the aorta (18, 47). Although the origin of reduced medial thickness lies within our manipulation of GRK2, the subsequent mechanisms of our unique aortic phenotype are currently unknown.

The mechanisms of increased GRK2 activity seen in the TgGRK2 and GRK2-C340S mouse are brought on differently. One is through transgenic overexpression, and the other is through loss of a negative regulatory mechanism, respectively. At this point, it is unknown whether SNO-GRK2 changes GRK2's interactome or whether it is gaining or losing interacting partners, aside from preventing β-arrestin recruitment. Therefore, it is debatable whether the loss of SNO-GRK2 may impact other protein functions that are relevant to CVD.

ACKNOWLEDGMENTS

We acknowledge Zuping Qu and Kevin Luu for all animal husbandry. Thank you to Maria Cimini, Ph.D. and Raj Kishore, Ph.D. for providing the immunohistochemistry protocol.

GRANTS

This work was supported by National Institutes of Health Grants F31-HL-142157 and T32-HL-091804 (to M. Lieu), R01-HL-105414 (to D. G. Tilley), R37-HL-061690 and P01-HL-075443 (to W. J. Koch), R01-DK-111042 (to R. Scalia), F30-HL-146007 (to M. Hoffman), and R01-HL-130218 (to K. Drosatos) and American Heart Association Grants 18MERIT33900036 (to W. J. Koch), 17POST33660942 (to C. de Lucia), and 18PRE34060115 (to M. Hoffman).

DISCLOSURES

No conflicts of interest, financial or otherwise, are declared by the authors.

AUTHOR CONTRIBUTIONS

M.L., C.J.T., J. Petovic, K.D., and W.J.K. conceived and designed research; M.L., C.J.T., C.d.L., M.P., R.R., J. Petovic, G.L., S.J.F., M.H., L.A.G., A.Y., and E.G. performed experiments; M.L., C.J.T., C.d.L., M.P., R.R., J. Petovic, G.L., S.J.F., M.H., L.A.G., and A.Y. analyzed data; M.L., C.J.T., C.d.L., J. Pfleger, M.P., S.J.F., M.H., L.A.G., R.S., D.G.T., and W.J.K. interpreted results of experiments; M.L., C.J.T., C.d.L., M.P., and G.L. prepared figures; M.L. drafted manuscript; M.L., C.d.L., J. Pfleger, S.E., R.S., D.G.T., and W.J.K. edited and revised manuscript; M.L. and W.J.K. approved final version of manuscript.

REFERENCES

1. **Agarwal M, Thomas P.** Prevalence of post-op. nosocomial infection in neurosurgical patients and associated risk factors—a prospective study of 2441 patients. *Nurs J India* 94: 197–198, 2003.
2. **Arani DT, Carleton RA.** Assessment of aortic valvular stenosis from the aortic pressure pulse. *Circulation* 36: 30–35, 1967. doi:10.1161/01.CIR.36.1.30.
3. **Benjamin EJ, Muntner P, Alonso A, Bittencourt MS, Callaway CW, Carson AP, Chamberlain AM, Chang AR, Cheng S, Das SR, Delling FN, Djousse L, Elkind MSV, Ferguson JF, Fornage M, Jordan LC, Khan SS, Kissela BM, Knutson KL, Kwan TW, Lackland DT, Lewis TT, Lichtman JH, Longenecker CT, Loop MS, Lutsey PL, Martin SS, Matsushita K, Moran AE, Mussolino ME, O'Flaherty M, Pandey A, Perak AM, Rosamond WD, Roth GA, et al.** Heart disease and stroke statistics—2019 update: a report from the American Heart Association. *Circulation* 139: e56–e528, 2019. doi:10.1161/CIR.0000000000000659.
4. **Biernacka A, Frangogiannis NG.** Aging and cardiac fibrosis. *Aging Dis* 2: 158–173, 2011.
5. **Bonacci TM, Mathews JL, Yuan C, Lehmann DM, Malik S, Wu D, Font JL, Bidlack JM, Smrcka AV.** Differential targeting of Gβγ-subunit signaling with small molecules. *Science* 312: 443–446, 2006. doi:10.1126/science.1120378.
6. **Brinks H, Boucher M, Gao E, Chuprun JK, Pesant S, Raake PW, Huang ZM, Wang X, Qiu G, Gumpert A, Harris DM, Eckhart AD, Most P, Koch WJ.** Level of G protein-coupled receptor kinase-2 determines myocardial ischemia/reperfusion injury via pro- and anti-apoptotic mechanisms. *Circ Res* 107: 1140–1149, 2010. doi:10.1161/CIRCRESAHA.110.221010.
7. **Casey LM, Pistner AR, Belmonte SL, Migdalovich D, Stolpnik O, Nwakanma FE, Vorobiof G, Dunaevsky O, Matavel A, Lopes CM, Smrcka AV, Blaxall BC.** Small molecule disruption of Gβγ signaling inhibits the progression of heart failure. *Circ Res* 107: 532–539, 2010. doi:10.1161/CIRCRESAHA.110.217075.
8. **Choi DJ, Koch WJ, Hunter JJ, Rockman HA.** Mechanism of β-adrenergic receptor desensitization in cardiac hypertrophy is increased β-adrenergic receptor kinase. *J Biol Chem* 272: 17223–17229, 1997. doi:10.1074/jbc.272.27.17223.
9. **Ciccarelli M, Sorriento D, Franco A, Fusco A, Del Giudice C, Annunziata R, Cipolletta E, Monti MG, Dorn GW 2nd, Trimarco B, Iaccarino G.** Endothelial G protein-coupled receptor kinase 2 regulates vascular homeostasis through the control of free radical oxygen species. *Arterioscler Thromb Vasc Biol* 33: 2415–2424, 2013. doi:10.1161/ATVBAHA.113.302262.
10. **Cimini M, Garikipati VNS, de Lucia C, Cheng Z, Wang C, Truongcao MM, Lucchese AM, Roy R, Benedict C, Goukassian DA, Koch WJ, Kishore R.** Podoplanin neutralization improves cardiac remodeling and function after acute myocardial infarction. *JCI Insight* 4: e126967, 2019. doi:10.1172/jci.insight.126967.
11. **Cohn HI, Harris DM, Pesant S, Pfeiffer M, Zhou RH, Koch WJ, Dorn GW II, Eckhart AD.** Inhibition of vascular smooth muscle G protein-coupled receptor kinase 2 enhances α_{1D}-adrenergic receptor constriction. *Am J Physiol Heart Circ Physiol* 295: H1695–H1704, 2008. doi:10.1152/ajpheart.00564.2008.
12. **Coresh J, Wei GL, McQuillan G, Brancati FL, Levey AS, Jones C, Klag MJ.** Prevalence of high blood pressure and elevated serum creatinine level in the United States: findings from the third National Health and Nutrition Examination Survey (1988-1994). *Arch Intern Med* 161: 1207–1216, 2001. doi:10.1001/archinte.161.9.1207.

13. **Crimmins E, Vasunilashorn S, Kim JK, Alley D.** Biomarkers related to aging in human populations. *Adv Clin Chem* 46: 161–216, 2008. doi:10.1016/S0065-2423(08)00405-8.
14. **Dai DF, Santana LF, Vermulst M, Tomazela DM, Emond MJ, MacCoss MJ, Gollahon K, Martin GM, Loeb LA, Ladiges WC, Rabinovitch PS.** Overexpression of catalase targeted to mitochondria attenuates murine cardiac aging. *Circulation* 119: 2789–2797, 2009. doi:10.1161/CIRCULATIONAHA.108.822403.
15. **Dai Z, Aoki T, Fukumoto Y, Shimokawa H.** Coronary perivascular fibrosis is associated with impairment of coronary blood flow in patients with non-ischemic heart failure. *J Cardiol* 60: 416–421, 2012. doi:10.1016/j.jjcc.2012.06.009.
16. **de Lucia C, Eguchi A, Koch WJ.** New insights in cardiac β-adrenergic signaling during heart failure and aging. *Front Pharmacol* 9: 904, 2018. doi:10.3389/fphar.2018.00904.
17. **de Lucia C, Wallner M, Eaton DM, Zhao H, Houser SR, Koch WJ.** Echocardiographic strain analysis for the early detection of left ventricular systolic/diastolic dysfunction and dyssynchrony in a mouse model of physiological aging. *J Gerontol A Biol Sci Med Sci* 74: 455–461, 2019. doi:10.1093/gerona/gly139.
18. **Dunnill MS.** Histology of the aorta in coarctation. *J Pathol Bacteriol* 78: 203–207, 1959. doi:10.1002/path.1700780122.
19. **Dutta S, Sengupta P.** Men and mice: relating their ages. *Life Sci* 152: 244–248, 2016. doi:10.1016/j.lfs.2015.10.025.
20. **Dzimiri N, Muiya P, Andres E, Al-Halees Z.** Differential functional expression of human myocardial G protein receptor kinases in left ventricular cardiac diseases. *Eur J Pharmacol* 489: 167–177, 2004. doi:10.1016/j.ejphar.2004.03.015.
21. **Eckhart AD, Ozaki T, Tevaearai H, Rockman HA, Koch WJ.** Vascular-targeted overexpression of G protein-coupled receptor kinase-2 in transgenic mice attenuates beta-adrenergic receptor signaling and increases resting blood pressure. *Mol Pharmacol* 61: 749–758, 2002. doi:10.1124/mol.61.4.749.
22. **Ferrara N, Komici K, Corbi G, Pagano G, Furgi G, Rengo C, Femminella GD, Leosco D, Bonaduce D.** β-adrenergic receptor responsiveness in aging heart and clinical implications. *Front Physiol* 4: 396, 2014. doi:10.3389/fphys.2013.00396.
23. **Flurkey KC, Currer JM, Harrison DE.** The mouse in aging research: American College laboratory animal medicine. In: *The Mouse in Biomedical Research* (2nd ed.), edited by Fox JG. Burlington, MA: Elsevier, 2007, p. 637–672.
24. **Geng X, Hwang J, Ye J, Shih H, Coulter B, Naudin C, Jun K, Sievers R, Yeghiazarians Y, Lee RJ, Boyle AJ.** Aging is protective against pressure overload cardiomyopathy via adaptive extracellular matrix remodeling. *Am J Cardiovasc Dis* 7: 72–82, 2017.
25. **Groen BB, Hamer HM, Snijders T, van Kranenburg J, Frijns D, Vink H, van Loon LJ.** Skeletal muscle capillary density and microvascular function are compromised with aging and type 2 diabetes. *J Appl Physiol (1985)* 116: 998–1005, 2014. doi:10.1152/japplphysiol.00919.2013.
26. **Gupta TC, Wiggers CJ.** Basic hemodynamic changes produced by aortic coarctation of different degrees. *Circulation* 3: 17–31, 1951. doi:10.1161/01.CIR.3.1.17.
27. **Huang ZM, Gao E, Fonseca FV, Hayashi H, Shang X, Hoffman NE, Chuprun JK, Tian X, Tilley DG, Madesh M, Lefer DJ, Stamler JS, Koch WJ.** Convergence of G protein-coupled receptor and S-nitrosylation signaling determines the outcome to cardiac ischemic injury. *Sci Signal* 6: ra95, 2013. doi:10.1126/scisignal.2004225.
28. **Iaccarino G, Barbato E, Cipolletta E, De Amicis V, Margulies KB, Leosco D, Trimarco B, Koch WJ.** Elevated myocardial and lymphocyte GRK_2 expression and activity in human heart failure. *Eur Heart J* 26: 1752–1758, 2005. doi:10.1093/eurheartj/ehi429.
29. **Iaccarino G, Dolber PC, Lefkowitz RJ, Koch WJ.** β-Adrenergic receptor kinase-1 levels in catecholamine-induced myocardial hypertrophy: regulation by β- but not α_1-adrenergic stimulation. *Hypertension* 33: 396–401, 1999. doi:10.1161/01.HYP.33.1.396.
30. **Isoyama S, Wei JY, Izumo S, Fort P, Schoen FJ, Grossman W.** Effect of age on the development of cardiac hypertrophy produced by aortic constriction in the rat. *Circ Res* 61: 337–345, 1987. doi:10.1161/01.RES.61.3.337.
31. **Kamal FA, Mickelsen DM, Wegman KM, Travers JG, Moalem J, Hammes SR, Smrcka AV, Blaxall BC.** Simultaneous adrenal and cardiac g-protein-coupled receptor-gβγ inhibition halts heart failure progression. *J Am Coll Cardiol* 63: 2549–2557, 2014. doi:10.1016/j.jacc.2014.02.587.
32. **Koch WJ, Rockman HA, Samama P, Hamilton RA, Bond RA, Milano CA, Lefkowitz RJ.** Cardiac function in mice overexpressing the beta-adrenergic receptor kinase or a beta ARK inhibitor. *Science* 268: 1350–1353, 1995. doi:10.1126/science.7761854.
34. **Lakatta EG.** So! What's aging? Is cardiovascular aging a disease? *J Mol Cell Cardiol* 83: 1–13, 2015. doi:10.1016/j.yjmcc.2015.04.005.
35. **Lakatta EG.** The reality of getting old. *Nat Rev Cardiol* 15: 499–500, 2018. doi:10.1038/s41569-018-0068-y.
36. **Leosco D, Iaccarino G, Cipolletta E, De Santis D, Pisani E, Trimarco V, Ferrara N, Abete P, Sorriento D, Rengo F, Trimarco B.** Exercise restores β-adrenergic vasorelaxation in aged rat carotid arteries. *Am J Physiol Heart Circ Physiol* 285: H369–H374, 2003. doi:10.1152/ajpheart.00019.2003.
37. **Levy D, Garrison RJ, Savage DD, Kannel WB, Castelli WP.** Prognostic implications of echocardiographically determined left ventricular mass in the Framingham Heart Study. *N Engl J Med* 322: 1561–1566, 1990. doi:10.1056/NEJM199005313222203.
38. **Li Y, Choi WJ, Wei W, Song S, Zhang Q, Liu J, Wang RK.** Aging-associated changes in cerebral vasculature and blood flow as determined by quantitative optical coherence tomography angiography. *Neurobiol Aging* 70: 148–159, 2018. doi:10.1016/j.neurobiolaging.2018.06.017.
39. **Lieu M, Koch WJ.** GRK2 and GRK5 as therapeutic targets and their role in maladaptive and pathological cardiac hypertrophy. *Expert Opin Ther Targets* 23: 201–214, 2019. doi:10.1080/14728222.2019.1575363.
40. **Liu M, Li XC, Lu L, Cao Y, Sun RR, Chen S, Zhang PY.** Cardiovascular disease and its relationship with chronic kidney disease. *Eur Rev Med Pharmacol Sci* 18: 2918–2926, 2014.
41. **Lymperopoulos A, Rengo G, Funakoshi H, Eckhart AD, Koch WJ.** Adrenal GRK2 upregulation mediates sympathetic overdrive in heart failure. *Nat Med* 13: 315–323, 2007. doi:10.1038/nm1553.
42. **Lymperopoulos A, Rengo G, Koch WJ.** Adrenergic nervous system in heart failure: pathophysiology and therapy. *Circ Res* 113: 739–753, 2013. [Erratum in *Circ Res* 119: e38, 2016]. doi:10.1161/CIRCRESAHA.113.300308.
43. **Maizel J, Xavier S, Chen J, Lin CH, Vasko R, Goligorsky MS.** Sirtuin 1 ablation in endothelial cells is associated with impaired angiogenesis and diastolic dysfunction. *Am J Physiol Heart Circ Physiol* 307: H1691–H1704, 2014. doi:10.1152/ajpheart.00281.2014.
44. **Mathar I, Vennekens R, Meissner M, Kees F, Van der Mieren G, Camacho Londoño JE, Uhl S, Voets T, Hummel B, van den Bergh A, Herijgers P, Nilius B, Flockerzi V, Schweda F, Freichel M.** Increased catecholamine secretion contributes to hypertension in TRPM4-deficient mice. *J Clin Invest* 120: 3267–3279, 2010. doi:10.1172/JCI41348.
45. **Mattace-Raso FU, van der Cammen TJ, Hofman A, van Popele NM, Bos ML, Schalekamp MA, Asmar R, Reneman RS, Hoeks AP, Breteler MM, Witteman JC.** Arterial stiffness and risk of coronary heart disease and stroke: the Rotterdam Study. *Circulation* 113: 657–663, 2006. doi:10.1161/CIRCULATIONAHA.105.555235.
46. **Montó F, Oliver E, Vicente D, Rueda J, Agüero J, Almenar L, Ivorra MD, Barettino D, D'Ocon P.** Different expression of adrenoceptors and GRKs in the human myocardium depends on heart failure etiology and correlates to clinical variables. *Am J Physiol Heart Circ Physiol* 303: H368–H376, 2012. doi:10.1152/ajpheart.01061.2011.
47. **Mourino-Alvarez L, Baldan-Martin M, Sastre-Oliva T, Martin-Lorenzo M, Maroto AS, Corbacho-Alonso N, Rincon R, Martin-Rojas T, Lopez-Almodovar LF, Alvarez-Llamas G, Vivanco F, Padial LR, de la Cuesta F, Barderas MG.** A comprehensive study of calcific aortic stenosis: from rabbit to human samples. *Dis Model Mech* 11: dmm033423, 2018. doi:10.1242/dmm.033423.
48. **Obrenovich ME, Smith MA, Siedlak SL, Chen SG, de la Torre JC, Perry G, Aliev G.** Overexpression of GRK2 in Alzheimer disease and in a chronic hypoperfusion rat model is an early marker of brain mitochondrial lesions. *Neurotox Res* 10: 43–56, 2006. doi:10.1007/BF03033333.
49. **Penela P, Murga C, Ribas C, Lafarga V, Mayor F Jr.** The complex G protein-coupled receptor kinase 2 (GRK2) interactome unveils new physiopathological targets. *Br J Pharmacol* 160: 821–832, 2010. doi:10.1111/j.1476-5381.2010.00727.x.
50. **Pleger ST, Harris DM, Shan C, Vinge LE, Chuprun JK, Berzins B, Pleger W, Druckman C, Völkers M, Heierhorst J, Øie E, Remppis A, Katus HA, Scalia R, Eckhart AD, Koch WJ, Most P.** Endothelial S100A1 modulates vascular function via nitric oxide. *Circ Res* 102: 786–794, 2008. doi:10.1161/CIRCRESAHA.108.172031.

51. **Raake PW, Schlegel P, Ksienzyk J, Reinkober J, Barthelmes J, Schinkel S, Pleger S, Mier W, Haberkorn U, Koch WJ, Katus HA, Most P, Müller OJ.** AAV6.βARKct cardiac gene therapy ameliorates cardiac function and normalizes the catecholaminergic axis in a clinically relevant large animal heart failure model. *Eur Heart J* 34: 1437–1447, 2013. doi:10.1093/eurheartj/ehr447.
52. **Raake PW, Vinge LE, Gao E, Boucher M, Rengo G, Chen X, DeGeorge BR Jr, Matkovich S, Houser SR, Most P, Eckhart AD, Dorn GW 2nd, Koch WJ.** G protein-coupled receptor kinase 2 ablation in cardiac myocytes before or after myocardial infarction prevents heart failure. *Circ Res* 103: 413–422, 2008. doi:10.1161/CIRCRESAHA.107.168336.
53. **Rengo G, Lymperopoulos A, Zincarelli C, Donniacuo M, Soltys S, Rabinowitz JE, Koch WJ.** Myocardial adeno-associated virus serotype 6–βARKct gene therapy improves cardiac function and normalizes the neurohormonal axis in chronic heart failure. *Circulation* 119: 89–98, 2009. doi:10.1161/CIRCULATIONAHA.108.803999.
54. **Rosen BD, Edvardsen T, Lai S, Castillo E, Pan L, Jerosch-Herold M, Sinha S, Kronmal R, Arnett D, Crouse JR 3rd, Heckbert SR, Bluemke DA, Lima JA.** Left ventricular concentric remodeling is associated with decreased global and regional systolic function: the Multi-Ethnic Study of Atherosclerosis. *Circulation* 112: 984–991, 2005. doi:10.1161/CIRCULATIONAHA.104.500488.
55. **Said MA, Eppinga RN, Lipsic E, Verweij N, van der Harst P.** Relationship of arterial stiffness index and pulse pressure with cardiovascular disease and mortality. *J Am Heart Assoc* 7: e007621, 2018. doi:10.1161/JAHA.117.007621.
56. **Sato PY, Chuprun JK, Schwartz M, Koch WJ.** The evolving impact of g protein-coupled receptor kinases in cardiac health and disease. *Physiol Rev* 95: 377–404, 2015. doi:10.1152/physrev.00015.2014.
57. **Schlegel P, Reinkober J, Meinhardt E, Tscheschner H, Gao E, Schumacher SM, Yuan A, Backs J, Most P, Wieland T, Koch WJ, Katus HA, Raake PW.** G protein-coupled receptor kinase 2 promotes cardiac hypertrophy. *PLoS One* 12: e0182110, 2017. doi:10.1371/journal.pone.0182110.
58. **Schumacher SM, Gao E, Cohen M, Lieu M, Chuprun JK, Koch WJ.** A peptide of the RGS domain of GRK2 binds and inhibits Gα(q) to suppress pathological cardiac hypertrophy and dysfunction. *Sci Signal* 9: ra30, 2016. doi:10.1126/scisignal.aae0549.
59. **Schumacher SM, Gao E, Zhu W, Chen X, Chuprun JK, Feldman AM, Tesmer JJ, Koch WJ.** Paroxetine-mediated GRK2 inhibition reverses cardiac dysfunction and remodeling after myocardial infarction. *Sci Transl Med* 7: 277ra31, 2015. doi:10.1126/scitranslmed.aaa0154.
60. **Schutzer WE, Reed JF, Blizniotes M, Mader SL.** Upregulation of G protein-linked receptor kinases with advancing age in rat aorta. *Am J Physiol Regul Integr Comp Physiol* 280: R897–R903, 2001. doi:10.1152/ajpregu.2001.280.3.R897.
61. **Schwartzkopff B, Mundhenke M, Strauer BE.** Alterations of the architecture of subendocardial arterioles in patients with hypertrophic cardiomyopathy and impaired coronary vasodilator reserve: a possible cause for myocardial ischemia. *J Am Coll Cardiol* 31: 1089–1096, 1998. doi:10.1016/S0735-1097(98)00036-9.
62. **Shi Y, Shu ZJ, Wang H, Barnes JL, Yeh CK, Ghosh PM, Katz MS, Kamat A.** Altered expression of hepatic β-adrenergic receptors in aging rats: implications for age-related metabolic dysfunction in liver. *Am J Physiol Regul Integr Comp Physiol* 314: R574–R583, 2018. doi:10.1152/ajpregu.00372.2017.
63. **Sonntag WE, Lynch CD, Cooney PT, Hutchins PM.** Decreases in cerebral microvasculature with age are associated with the decline in growth hormone and insulin-like growth factor 1. *Endocrinology* 138: 3515–3520, 1997. doi:10.1210/endo.138.8.5330.
64. **Sopko NA, Turturice BA, Becker ME, Brown CR, Dong F, Popović ZB, Penn MS.** Bone marrow support of the heart in pressure overload is lost with aging. *PLoS One* 5: e15187, 2010. doi:10.1371/journal.pone.0015187.
65. **Sorriento D, Santulli G, Franco A, Cipolletta E, Napolitano L, Gambardella J, Gomez-Monterrey I, Campiglia P, Trimarco B, Iaccarino G, Ciccarelli M.** Integrating GRK2 and NFkappaB in the pathophysiology of cardiac hypertrophy. *J Cardiovasc Transl Res* 8: 493–502, 2015. doi:10.1007/s12265-015-9646-0.

65a. **The Jackson Laboratory.** *Biology of the Laboratory Mouse* (2nd ed.), edited by Green EL. New York: Dover Publications, 1966.

66. **Whalen EJ, Foster MW, Matsumoto A, Ozawa K, Violin JD, Que LG, Nelson CD, Benhar M, Keys JR, Rockman HA, Koch WJ, Daaka Y, Lefkowitz RJ, Stamler JS.** Regulation of beta-adrenergic receptor signaling by S-nitrosylation of G-protein-coupled receptor kinase 2. *Cell* 129: 511–522, 2007. doi:10.1016/j.cell.2007.02.046.
67. **White DC, Hata JA, Shah AS, Glower DD, Lefkowitz RJ, Koch WJ.** Preservation of myocardial β-adrenergic receptor signaling delays the development of heart failure after myocardial infarction. *Proc Natl Acad Sci USA* 97: 5428–5433, 2000. doi:10.1073/pnas.090091197.
68. **Xu X, Wang B, Ren C, Hu J, Greenberg DA, Chen T, Xie L, Jin K.** Age-related impairment of vascular structure and functions. *Aging Dis* 8: 590–610, 2017. doi:10.14336/AD.2017.0430.
69. **Yildiran T, Koc M, Bozkurt A, Sahin DY, Unal I, Acarturk E.** Low pulse pressure as a predictor of death in patients with mild to advanced heart failure. *Tex Heart Inst J* 37: 284–290, 2010.
70. **Ytrehus K, Hulot JS, Perrino C, Schiattarella GG, Madonna R.** Perivascular fibrosis and the microvasculature of the heart. Still hidden secrets of pathophysiology? *Vascul Pharmacol* 107: 78–83, 2018. doi:10.1016/j.vph.2018.04.007.
71. **Zheng F, Plati AR, Potier M, Schulman Y, Berho M, Banerjee A, Leclercq B, Zisman A, Striker LJ, Striker GE.** Resistance to glomerulosclerosis in B6 mice disappears after menopause. *Am J Pathol* 162: 1339–1348, 2003. doi:10.1016/S0002-9440(10)63929-6.